THE SPECIFIC CUTTING ENERGY ON THE CUTTING EDGES OF A THE COMBINED DRILLING/THREAD MILLING PROCESS: THRILLING

Anna Carla Araujo, M B G Jun

THE SPECIFIC CUTTING ENERGY ON THE CUTTING EDGES OF A THE COMBINED DRILLING/THREAD MILLING PROCESS: THRILLING

A.C. Araujo [1*], M.B.G. Jun [2]
[1] Department of Mechanical Engineering, CEFET/RJ, Rio de Janeiro, RJ, Brazil
[2] Department of Mechanical Engineering, University of Victoria, British Columbia, Canada
*annaaraujo@cefet-rj.br

Abstract
This paper investigates the specific energy and the chip load of a thread making process called thrilling, which performs both drilling and thread milling with one tool. A chip thickness and cutting force models have been used for a drilling operation with a thrilling tool. The models consider a complex geometry of a thrilling tool and the unique tool paths associated with the drilling operation and thread milling operation with a thrilling tool. Calibration experiments have been conducted to estimate the cutting coefficients associated with specific cutting energies and the relation between the specific cutting energies of both operations has been compared.

1. INTRODUCTION

Threads on a workpiece can be produced in a variety of ways based on two basic principles: plastic working and metal cutting. Threads made by plastic working are stronger but lack the accuracy required for many applications. Threads made by cutting, on the other hand, provide better accuracy and finish and threads can be made even with brittle materials. There are two common cutting processes for internal thread generation: cut tapping and thread milling. Recently, a thread cutting tool called a thriller has been developed [1], which can perform both drilling and thread cutting operations. Thus, after drilling a hole, no tool change is required to make threads, leading rapid thread generation. This elimination of tool change times leads to decreases in tooling cost and increase in process flexibility and material savings. One substantial disadvantage of the process may be its low length to diameter (L/D) ratio capability due to tool deflection and vibration. Also, the very bottom of a blind hole will not have threads due to the unique design of the thrilling tool. However, little is known about the process mechanics, and this process needs to be understood for effective application of the process.

The bottom of a thrilling tool (thriller) is similar to a drill, and along the helix of the tool has the tool geometry of a thread milling tool. Since one tool performs two different processes consecutively, the geometry of the tool and the mechanics of the process are unique. The quality of the threads generated would depend on the unique characteristics of the tool and the process. However, though thread making processes both based on plastic working [2-5] and thread cutting [6-8] have been extensively studied by many researchers, the thrilling process has not been so investigated. The thrilling process has been experimentally investigated recently [8-9]. However, no modeling work has been conducted to understand the thread milling operation during the thrilling process.

The objective of this paper is to analyze the cutting energies in both processes on the same tool and machining the same material. The model is based on chip thickness and cutting force model in order to study and predict the performance of the thrilling process as it relates to thread quality. The model considers the complex geometry of a thrilling tool and the unique tool paths associated with the operation done by a thriller. Cutting forces during thrilling are measured and related to the cutting characteristics of the process. Calibration experiments have been conducted to estimate the cutting coefficients associated with specific cutting energies. Experiments have been conducted to validate the developed model.

2. PROCESS DESCRIPTION AND TOOL GEOMETRY

2.1 Description of a Thrilling Process

The machining process of thrilling can be divided into seven stages as shown in Figure 1 [10]. The first stage involves positioning the tool above the workpiece where the hole with threads needs to be made. Once the tool is positioned, it drills down into the workpiece to the desired depth of the hole. Then, the tool retracts up enough so that the cutting lips do

not interfere with the thread milling operation. In order to make the thread, while rotating at the prescribed rotational speed and retracting the tool half the pitch, the tool moves radially into the workpiece to a proper radial depth of cut through a helical “run-in loop”. Once the cutting edge is engaged into the workpiece at the desired radial depth of cut, the tool moves one complete revolution around the hole in a planetary gear motion, simultaneously moving up helically. The number of threads generated in this one revolution corresponds to the number of threads engaged in the workpiece. Then, the tool moves back to the center of the hole, and, finally, the tool is retracted out of the hole.

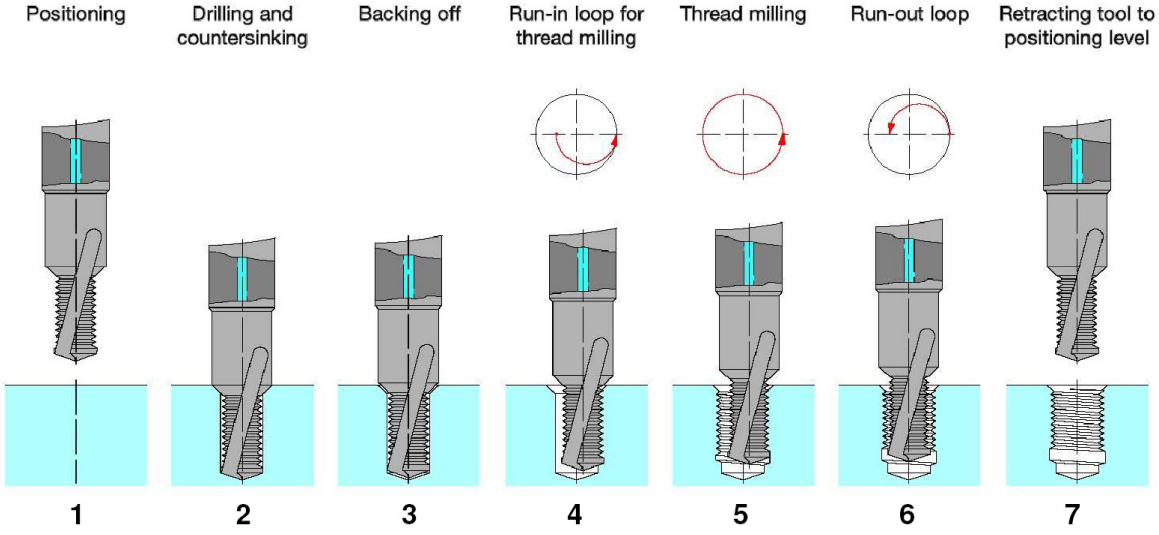

Figure 1: The complete Thrilling process: Drilling, End Milling and Thread Milling Operations

2.2 Thrilling Tool Geometry

The geometry of a thriller is shown in Figure 2. Each flute has a chisel edge, drilling cutting lip, milling cutting edge, and thread milling cutting edge. The chisel edge does not cut but only spreads the material sideways by an indentation mechanism [11]. It has a width of 2w and an edge angle of ψc. The cutting lips have an offset from the center of the tool due to the chisel edge. The cutting lips remove the material with a constant chip thickness as the tool is fed into the workpiece at a feed rate of fd. The chisel edge and cutting lips have the shape of a drill. The cutting lips at the point angle κ and with the height hd meet with the milling cutting edge. The milling cutting edge height is denoted as hm.

The milling cutting edge separates the drilling part from the thread milling part. During the drilling stage, the milling cutting edge does not cut but only acts as a helical flute for chip evacuation. Then, the milling cutting edge cuts as a milling tool so that the drilling cutting lips do not interfere with the thread milling operation. During the thread milling operation, the cutting forces generated include the forces due to thread making and also cutting by this milling cutting edge. The external diameter of the thread milling cutting edge is smaller than the milling cutting edge diameter (dm).

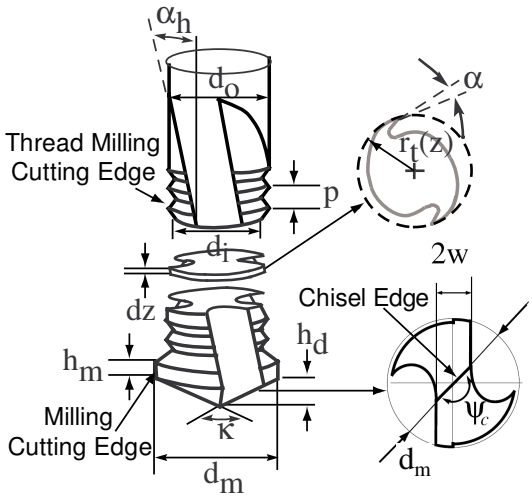

Figure 2: A thrilling tool geometry and discretization

The threads on a thriller have the maximum diameter on the outside do and minimum diameter di, which can be obtained as di = do – 2ht, where ht is the thread height. The thread pitch is denoted as p.

The thread milling tool can be analyzed as a stack of disks, 1...Nz, where each disk has dz thickness and a variable radius rt(z) as shown in Figure 2. The variable diameter rt(z) can be written as a function of the disk height z

measured from the bottom of the tool. The radius of each disk element rt(z) can be obtained as

$$r_t(z)=\begin{cases} z\,r_m/h_d & \text{if } 0<z\le h_d \\ r_m & \text{if } h_d<z\le h_{dm} \\ r_i+3h_m(h_p-z)/p & \text{if } h_{dm}<z\le h_p \\ r_i & \text{if } nt(z_p)=0,3,6,.. \\ r_i+3h_t(z_p-nt(z_p/3)p-p/3)/p & \text{if } nt(z_p)=1,4,7,.. \\ r_i+3h_t(p-z_p-nt(z_p/3)p)/p & \text{if } nt(z_p)=2,5,8,.. \end{cases} \quad (1)$$

where $z_p = z - h_p$, $h_p = h_d + h_m + 3/p$, $h_{dm} = h_d + h_m$, and the function $nt(\xi)$ is defined as

$$nt(\xi) = IntegerPart\left(\frac{3\xi}{p}\right) \quad (2)$$

As will be shown later, this variation in the disk diameter along the tool causes radial depth of cut to vary for each disk. The angle between the flutes depends on the numbers of flutes N_f and is defined by the tool geometry as

$$\theta_p = \frac{2\pi}{N_f} \quad (3)$$

3. DRILLING WITH A THRILLING TOOL

3.1 Drilling Process

Since the bottom geometry of a thriller for drilling share the same geometry of a typical drill, as can be seen in Figure 3, the cutting mechanics is the same as in normal drilling. Nevertheless, there is an additional force during the drilling process due to the friction of the end milling edge with the drilled hole, which will be neglected in this study.

The drilling process has been studied by many researchers and chip thickness and force models have been developed for drilling [12-16].

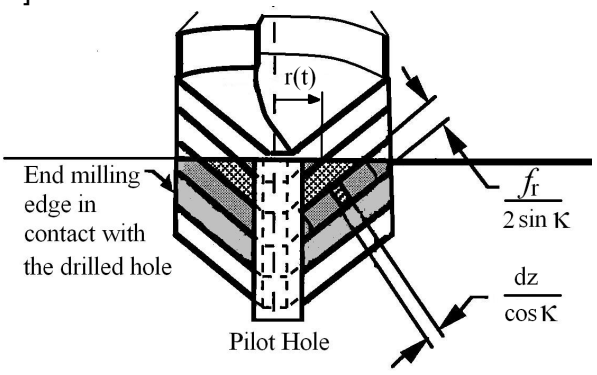

Figure 3: Drilling Chip Load

As it is important to control the entry of the tool, a pilot hole is needed. The pilot hole has radio rp and it is bigger then the web thickness, and so the chisel edge force is acting in the process. The cutting force increases as the tool feeds until the driilling cutting edge enters the material. It varies linealy and there is a first step when the pilot hole is present and a second step where there is no more pilot hole and the tool is fully engaged. The thrust force is described as:

$$F_z = 2\cdot\int K_z\cdot t_c\cdot db \quad (4)$$

$$t_c = \frac{f}{2}\cdot\sin(\kappa) \quad (5)$$

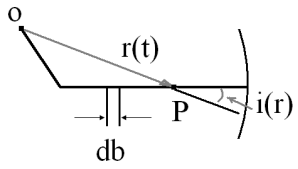

Figure 4: Drilling Inclination Angle

$$db = \cos(i(r))dr \quad (6)$$

$$F_z = 2\cdot\int_{rp}^{r(t)} K_n\cdot\frac{f}{2}\cdot\sin(\kappa)\cdot\cos(i(r))\cdot dr \quad (7)$$

Where r(t) is the radio of the external point of the drilling cutting edge in contact with the workpiece, i(r,t) is the inclinatiion angle of each point of the drilling cutting edge and Kn is the specific cutting energy of this point.

$$\sin(i) = \frac{w}{r(t)}\cdot\sin(\kappa) \quad (8)$$

The amplitude of the thrust force in first step ($A_1[F_z]$), when the tool is fully inside the workpiece and still the chisel edge is not in contact with the material due to the pilot hole, the force can be written as:

$$A_1[F_z] = 2\cdot\int_{rp}^{\frac{dm}{2}} K_n(r)\cdot\frac{f}{4}\cdot\sin(\kappa)\cdot\left[2-\left(\frac{w}{r(t)}\cdot\sin(\kappa)\right)^2\right]\cdot dr \quad (9)$$

The torque can be written as:

$$T = 2\cdot\int_{rp}^{r(t)} K_t\cdot\frac{f}{2}\cdot r(t)\cdot\sin(\kappa)\cdot\cos(i(r))\cdot dr \quad (10)$$

Calculating the first step of Torque:

$$A_1[T] = \int_{rp}^{\frac{dm}{2}} K_t(r)\cdot r\cdot\frac{f}{4}\cdot\sin(\kappa)\cdot\left[2-\left(\frac{w}{r(t)}\cdot\sin(\kappa)\right)^2\right]\cdot dr \quad (11)$$

Where Kt(r) is the specific energy for the point. After the tool passes to the pilot hole, the force and the torque acquire another stage that combine the force due to the chisel edge and the cutting edge. For the purpose of this work, that is calculating the specific pressure of the processes, it will not be calculated.

3.2 Specific Energies on Drilling

The specific energy in drilling was investigated by [15] and experimentally found that:

$$K_n(r) = C\cdot\left(\frac{2\cdot r}{dm}\right)^a \rightarrow \overline{K_n} = \frac{1}{r*}\int_{ri}^{re} C\cdot\left(\frac{2\cdot r}{dm}\right)^a dr \quad (12)$$

$$K_t(r) = D\cdot\left(\frac{2\cdot r}{dm}\right)^b \rightarrow \overline{K_t} = \frac{1}{r*}\int_{ri}^{re} C\cdot\left(\frac{2\cdot r}{dm}\right)^a dr$$

Where C and D are dependant of the spindle speed and feed and a and b are only a function of the pair of tool and workpiece material.
In thrilling it is possible to calculate the specific pressure while the cutting is in progress and that is the contribution of this article.

4. END MILLING AND THREAD MILLING MODEL

As the thread milling operation in thrilling involves a unique tool path consisting of run-in, thread-milling, and run-out motions, an accurate modeling of the tool and cutting edge locations is important for chip thickness model development

4.1 Tool Path Generation and Cutting Descriptions

There are five different tool paths involved in the thread milling operation of the thrilling process (stages 4 to 6 in Figure 1). These five different paths are defined as: (1) pre-run-in from point O to J, (2) run-in from J to K, (3) thread milling from K to K itself passing through L and M, (4) run-out from C back to B, and (5) post-run-out to the initial position, as shown in Figure 6(a). The five paths in the three dimensional space are shown in Figure 6(b). For a specific time t, θt(t) indicates the angular location of the tool center with respect to the absolute X-Y-Z reference coordinate frame and θ(t) represents the angular rotation of the tool about its own axis (Figure 6(a)). Note that θt(t) and θ(t) are in the opposite directions. While the tool moves in the counter-clockwise direction, the tool rotates in the clockwise direction, resulting in climb milling during the thread milling operation. Note that, in this case, point B is located to the left of the X-Y axis. If the conventional milling is desired, the tool motion should be in the clockwise direction, provided that the tool rotates in the clockwise direction.

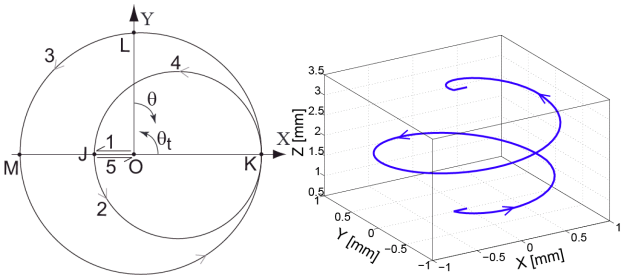

(a) (b)

Figure 5: Tool paths involved in thread milling operation

Once the tool retracts a third of the thread pitch p after drilling (stage 3 in Figure 1 at which no cutting occurs), it moves in the negative X-direction (path 1 Figure 6(a)) in by the distance of the difference between the milling cutting edge radius (rm) and the thread milling cutting edge outside radius (ro), i.e., rm – ro. Cutting starts during this motion only by the milling cutting edge. Cutting by the thread milling cutting edge starts subsequently during the half-circular, helical, run-in motion in the counter-clockwise direction (path 2 in Figure 4). The radius of the circular run-in motion (rin) is given as

$$r_{in} = r_m - r_o + \frac{h_t}{2}. \quad (13)$$

The circular motion at this radius ensures that the radial depth of cut gradually increases as the tool follows the run-in path, and at the end of the half-circular helical path, the thread is fully engaged in the workpiece, resulting in the radial depth of cut (dr) for the milling cutting edge as dr = ht + rm – ro and for the thread milling cutting edge as dr = rt(z) – ri. The tool moves up in the Z-direction half the pitch during the run-in motion.
During the thread milling stage (path 3 in Figure 4(a)), the tool moves helically for one complete revolution at the radius same as the radial depth of cut for the milling cutting edge (rth = dr = ht + rm – ro). The threads are generated in the workpiece during this stage. The cutting edges are fully engaged in the workpiece for

the first half of the revolution. However, for the second half, the thread milling cutting edges now cut the incomplete threads in the workpiece generated by the previous cutting edges during the run-in stage. The milling cutting edge cuts over these incomplete threads generated by the very bottom thread milling cutting edges. Thus, for the second half of the revolution, the radial depth of cut for each disk element of the cutting edge (as shown in Figure 2) gradually decreases.

The thread milling cutting edges do not cut during the run-out stage (path 4 in Figure 6(a)) because the cutting edges now follow the threads generated by the previous cutting edges. But, cutting occurs by the milling cutting edge as it cuts over the threads generated. The radius of curvature during the run-out motion is the same as that during the run-in motion (rout = rin). After the run-out stage, the tool moves back to the center (post-run-out motion) and no cutting occurs during this motion.

In order to determine the cutting edge positions for chip thickness development, the positions of the tool center (pcX(t), pcY(t), pcZ(t)) along the tool path during the thread milling are needed. For the tool paths from 2 to 4, θt(t) varies from π to 5π. For simplicity, the time variable will be suppressed from the equations. The tool center X and Y positions for paths 2 and 4 can be obtained as

$$p_{cX} = -(r_m - r_o) + r_{in}(1 + \cos\theta_t), \quad p_{cY} = r_{in}\sin\theta_t \tag{14}$$

and the X and Y positions for path 3 are given by

$$p_{cX} = r_{th}\cos\theta_t, \quad p_{cY} = r_{th}\sin\theta_t \,. \tag{15}$$

The Z position of the tool center for the paths 2 to 4 can be obtained from

$$p_{cZ} = h_t \frac{(\theta_t - \pi)}{2\pi} \,. \tag{16}$$

Tool center trajectory for the 5 paths is shown in Figure 6(b), and Figure 5 shows those of the cutting edges during the thread milling operation.

During the thread milling operation, as the tool rotates about its own axis and follows the tool paths described above, the tool center angular location (θ_t) and the rotational angle (θ) changes simultaneously. As shown in Figure 7 for an arbitrary disk element of a two-fluted tool, if the tool is initially at a given angular location ($\theta_{t,i}$) or at point *A* and the tool rotates by the amount of $\theta_p = 2\pi/N_f$ about its own axis, the tool center moves by the amount of the feed per tooth (f_t). Simultaneously, the tool center revolves around the center of the drilled hole and the new tool center angular location is denoted as $\theta_{t,i'}$. The position of the tool axis at the angular location $\theta_{t,i'}$ is represented by the point *A'*. Thus, the tool moves from point *A* to point *A'* after a half revolution and to point B after a complete revolution. The distance from *A* to *A'* is equal to the feed per tooth (f_t) and from *A* to *B* is equal to the feed per revolution (f_r). The coordinate frame *X-Y-Z* is the reference frame at the center of the drilled hole *O*, and the local coordinate frame for *B* is the *x-y-z* coordinate frame, which is a rotating frame. Figure 7 shows both coordinate frames and also shows the tangential (F_t) and radial (F_r) forces acting on the cutting edge at the rotational angle θ when the tool is at point *B*. The chip load taken by the cutting edge is indicated by the shaded region.

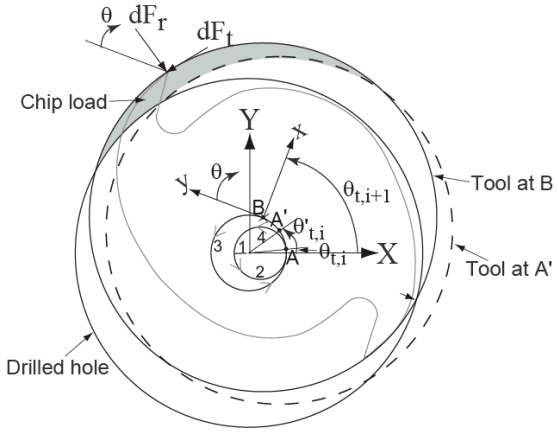

Figure 6: Chip load and coordinate frames during thread milling operation

Figure 6 shows the details of geometry parameters associated for chip thickness model development. The radius of the tool center location with respect to the *X-Y-Z* reference frame is denoted as r_c, and the radius of the hole surface for the disk element, represented by the line connecting the points *O* and *Q*, is denoted as $r_q(\theta_t, z+p)$. Note that initially, during the first two paths of the thread milling operation, the radius of the hole surface is equal to the radius of the milling cutting edge, i.e., $r_q = r_m$. However, during the third path, the cutting edge now cuts over the area previously cut during the first two paths. Figure 8 shows the area of cut during each path of the thread milling operation. As shown, starting from the point *D* during the third path, the cutting edge now cuts over the area cut from the previous paths. Thus, the radius of the hole surface $r_q(\theta_t, z)$ can be written as

$$r_q(\theta_t, z) = \begin{cases} r_m & \theta_t \le \dfrac{5\pi}{2} \\ r_t(z) + (r_m - r_i)\sin\left(\dfrac{\theta_t}{3} - \dfrac{\pi}{6}\right) & \dfrac{5\pi}{2} < \theta_t \le 4\pi \\ r_t(z) + (r_m - r_i) & \theta_t > 4\pi \end{cases} \quad (17)$$

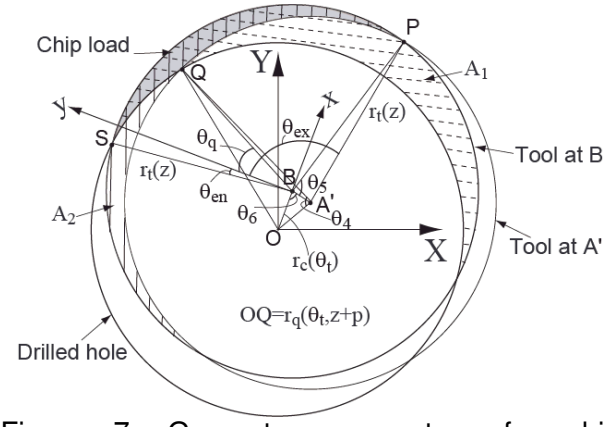

Figure 7: Geometry parameters for chip thickness model development

Note that because the paths from 2 to 4 are helical paths and thus the tool moves up as θ_t is increased, during the path 3, the cutting edge cuts over the surface previously cut by the cutting edge one pitch higher than the current. This is why the radius of the hole surface in Figure 7 is written as $r_q(\theta_t, z+p)$, where p is the thread pitch. After the path 3, the cutting edge does not cut but follows through the threads generated by the one-pitch-higher cutting edge. The only cutting edge that engages in cutting during the path 4 is the milling cutting edge because it is now positioned one pitch higher and cuts over the thread generated.

The points *P* and *S* in Figure 7 represent the entry point and exit point of the cutting edge. The chip load is taken between the entry and exit angles and it is the intersection of the hatched areas with solid and dashed line. The entry and exit angles can be written as

$$\theta_{en} = \theta_4 - \frac{\pi}{2}$$
$$\theta_{ex} = \frac{3\pi}{2} - \theta_5 - \theta_6 \quad (1)$$

where

$$\theta_4 = \cos^{-1}\left[\frac{r_c(\theta_t)^2 + r_t(z)^2 - r_q(\theta_t, z)^2}{2 r_c(\theta_t) r_t(z)}\right]$$
$$\theta_5 = \cos^{-1}\left[\frac{f_t}{2 r_t(z)}\right], \qquad \theta_6 = \cos^{-1}\left[\frac{f_t}{2 r_c(\theta_t)}\right]. \quad (18)$$

The maximum height of the hatched area with solid lines (A_2) is the feed per tooth (f_t) and the maximum height of the hatched area with dashed lines (A_1) is the radial depth of cut (d_r). The radial depth of cut is expressed as

$$d_r(\theta_t, z) = r_t(z) + r_c(\theta_t) - r_q(\theta_t, z + p), \quad (19)$$

and the chip thickness for the j^{th} tooth can be obtained as

$$tc(\theta_j, z) = \begin{cases} d_r(\theta_t, z)\sin\left(\dfrac{\pi(\theta_j - \theta_{en})}{\pi - 2\theta_{en}}\right) & \theta_{en} < \theta_j \le \theta_q \\ f_t \sin\left(\theta_j + \dfrac{\pi}{2} - \dfrac{\pi - 2\theta_6}{2}\right) & \theta_q < \theta_j \le \theta_{ex} \end{cases} \quad (20)$$

where

$$\theta_j = \theta - (j-1)\frac{2\pi}{N_f} - z\frac{\tan(\alpha_h)}{r_t(z)}. \quad (21)$$

4.2 Cutting Force Model Development

The tangential (dFt) and radial (dFr) cutting forces acting on a differential flute element with height dz, as shown in Figure 9, can be modeled as follows,

$$dF_t = K_t tc(\theta_j, z)dz$$
$$dF_r = K_r tc(\theta_j, z)dz$$
$$dF_z = K_z tc(\theta_j, z)dz \quad (22)$$

where K_t, K_r, and K_z [N/mm^2] are specific tangential, radial, and axial cutting constants or energies, which represent the energy required to shear or deform the workpiece. These coefficients need to be identified through experimental calibration. The tangential and radial forces can be transformed to the *x-y-z* rotating frame as

$$dF_x = -\left(K_r \sin\theta_j + K_t \cos\theta_j\right) tc(\theta_j, z)dz$$
$$dF_y = -\left(K_r \cos\theta_j - K_t \sin\theta_j\right) tc(\theta_j, z)dz. \quad (23)$$

The *X-Y* forces in the reference frame then can be expressed as

$$dF_X = dF_x \cos\theta_t - dF_y \sin\theta_t$$
$$dF_Y = dF_x \sin\theta_t + dF_y \cos\theta_t. \quad (24)$$

In order to determine the torque with respect to the reference frame, the forces acting on the cutting edge during the thread milling operation need to be examined carefully as shown in Figure 9. Considering the force components that are tangential to the hole being threaded,

the torque with respect to the reference frame can be computed as

$$dT_q = dF_t r_{tq}(\theta_t, z)\cos(\theta_{tq}) - dF_r r_{tq}(\theta_t, z)\sin(\theta_{tq}) \quad (25)$$

where

$$r_{tq} = \sqrt{r_c(\theta_t)^2 + r_t(z)^2 - 2r_c(\theta_t)r_t(z)\cos(\theta_j + \theta_t - \pi/2)}$$

$$\theta_{tq} = \sin^{-1}\left(\frac{r_c(\theta_t)\sin(\pi/2 + \theta_j)}{r_{tq}}\right).$$

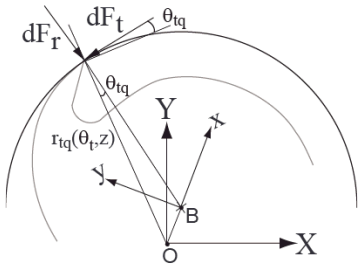

Figure 10: Forces acting on cutting edges with respect to the reference frame [9]

5. MODEL CALIBRATION

Drilling calibration tests were used to determine the cutting coefficients. On Figure 11 an experimental data is shown.

Experiments with the same material, Aluminum 6061, and the same thrilling tool were performed with 1000 rpm and 2000 rpm of spindle speed and 0.05 mm/rev and 0.15 mm/rev of feed rate (and its combination) and an additional experiment to calculate a and b coefficients (1500 rpm and 0.1 mm/rev).

The total cutting energies, $\overline{K_n}$, and $\overline{K_t}$, respectively, are represented by the following equations,

$$\ln(\overline{Kt}) = c_0 + c_1 \cdot \ln(f) + c_2 \cdot \ln(N)$$
$$\ln(\overline{Kr}) = d_0 + d_1 \cdot \ln(f) + d_2 \cdot \ln(N) \quad (26)$$

where $a_{0\text{-}2}$, and $b_{0\text{-}2}$ are cutting coefficients for the corresponding coefficients. The calibration values of cutting coefficient can be seen on Table 1.

Cutting coefficients for drilling			
c_0	5.0596	d_0	2.1888
c_1	0.0069	d_1	0.1383
c_2	-0.3193	d_2	-0.6040

Table 1. Calibrated values of cutting coefficients on drilling

The estimation of the specific cutting energies for thread milling was done to determinate the coefficients, shown on Equation 17.

$$\ln(K_t) = a_0 + a_1 \ln(f_t) + a_2 \ln(N)$$
$$\ln(K_r) = b_0 + b_1 \ln(f_t) + b_2 \ln(N)$$
$$\ln(K_z) = c_0 + c_1 \ln(f_t) + c_2 \ln(N) \quad (27)$$

where f_t is feed per tooth (mm/tooth) and N is the rotational speed (rpm), $a_{0\text{-}2}$, $b_{0\text{-}2}$, and $c_{0\text{-}2}$ are cutting coefficients for the thread milling corresponding cutting energies. Table 2 shows the results of the calibration and the values of the cutting coefficients for thread milling operation shown on Figure 12.

Table 2. Calibrated values of cutting coefficients on thread milling

Cutting coefficients for Thread Milling					
A_0	6.8750	b_0	6.5507	c_0	6.2346
B_1	-0.0142	c_1	0.0069		
B_2	0.2848	c_2	0.2323		

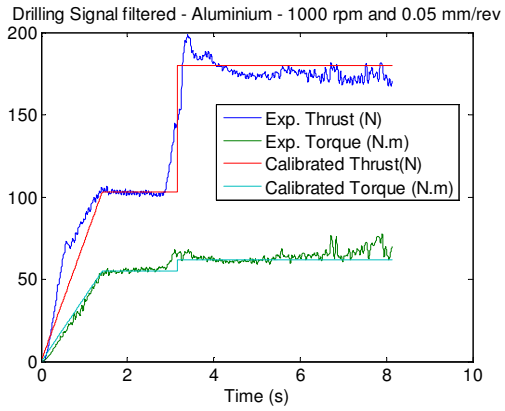

Figure 11: Drilling Experimental Data and comparison to simulation

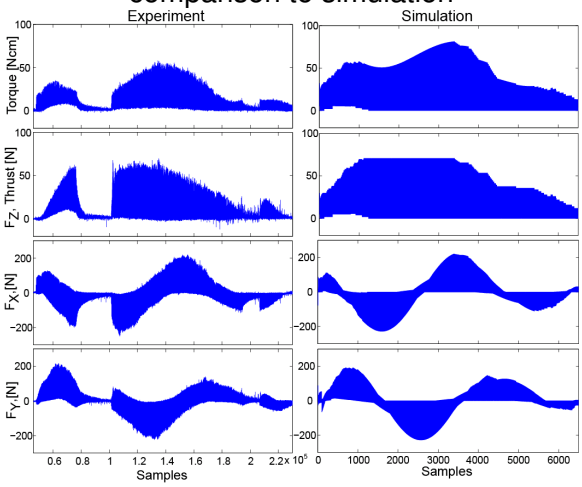

Figure 12: Comparison between experiment and simulation for validation when N = 1500 rpm and fr = 0.015 mm/rev for Thread Milling Operation

6. CONCLUSION

A combined drilling and thread milling operation called thrilling has been investigated and a chip thickness and cutting force model have been

developed for drilling and thread milling operation with a thrilling tool.
Calibration experiments have been conducted to estimate the cutting coefficients associated with specific cutting energies in drilling and Thread Milling processes with a Thrilling Tool
As the tool material and workpiece are the same in both operations, the drilling coefficient should give information about the thread milling velocities. A correlation between those coefficients need to be done as a future work.

7. ACKNOWLEDGMENTS

This research is based upon the work conducted at the Center of Machine Tools Systems Research at the University of Illinois at Urbana-Champaign (UIUC). The authors gratefully acknowledge the support of Shiv Kapoor and Richard DeVor at UIUC. The authors also acknowledge the support of Brazilian Research Councils CNPq and FAPERJ.

8. REFERENCES

[1] MMS Online (Modern Machine Shop Online), http://www.mmsonline.com/articles/019603.html.

[2] Cao, T. and Sutherland, J.W., 2002 "Investigation of thread tapping load characteristics through mechanistic modeling and experimentation," International Journal of Machine Tools and Manufacture, 42(14), pp. 1527-1538.

[3] Ivanina, I.V., 2005 "Influence of parameters of the cutting part of taps on threading accuracy," Measurement Techniques, 48(10), pp. 990-4.

[4] Warrington, C., Kapoor, S.G., and DeVor, R.E., 2005 "Experimental investigation of thread formation in form tapping," Journal of Manufacturing Science and Engineering, Transactions of the ASME, 127(4), pp. 829-836.

[5] Chowdhary, S., Kapoor, S.G., Ozdoganlar, O.B., and DeVor, R.E. 2002, "Modeling and analysis of internal thread forming," NAMRC XXX, May 21-24 2002, West Lafayette, ID.pp. 1-8.

[6] Dogra, A.P.S., Kapoor, S.G., and DeVor, R.E., 2002 "Mechanistic model for tapping process with emphasis on process faults and hole geometry," Journal of Manufacturing Science and Engineering, Transactions of the ASME, 124(1), pp. 18-25.

[7] Araujo, A.C., Silveira, J.S., Jun, M.B.G., Kapoor, S.G., and DeVor, R.E., 2006 "A model for thread milling cutting forces," International Journal of Machine Tools & Manufacture, 46, pp. 2057-2065.

[8] Araujo, A.C., Jun, M.B.G., Kapoor, S.G., and DeVor, R.E., 2007 "Experimental Investigation of a Combined Drilling and Thread Milling Process: Thrilling," Transactions of NAMRI/SME, XXXV, pp. 518-527.

[9] Jun, M.B.G. and Araujo, A.C., 2008 " Modeling and Analysis Of The Thread Milling Operation In The Combined Drilling/Thread Milling Process" - Proceedings of the 2008 International Manufacturing Science and Engineering Conference

[10]Emuge,www.emuge.com/carbide_thread/bgf.html.

[11] Altintas, Y., 2000, "Manufacturing Automation: Metal Cutting Mechanics, Machine Tool Vibrations, and CNC Design. 2000, Cambridge University Press.

[12] Furness, R.J., Wu, C.L., and Ulsoy, A.G. 1992, "Dynamic modeling of the thrust force and torque for drilling, Chicago, IL, USA.pp. 384-90.

[13] Strenkowski, J.S., Hsieh, C.C., and Shih, A.J., 2004 "An analytical finite element technique for predicting thrust force and torque in drilling," International Journal of Machine Tools & Manufacture, 44(12-13), pp. 1413-21.

[14] Yongping, G., Cheng, L., and Ehmann, K.F., 2005 "Dynamics of initial penetration in drilling: part 1-mechanistic model for dynamic forces," Transactions of the ASME. Journal of Manufacturing Science and Engineering, 127(2), pp. 280-8.

[15] Chandrasekharan, V., Kapoor, S.G., and DeVor, R.E., 1998 "Mechanistic model to predict the cutting force system for arbitrary drill point geometry," Journal of Manufacturing Science and Engineering, Transactions of the ASME, 120(3), pp. 563-570.

[16] Altintas, Y. and Weck, M., 2004 "Chatter stability of metal cutting and grinding," CIRP Annals - Manufacturing Technology, 53(2), pp. 619-642.